

Near-Field Investigations of the Landers Earthquake Sequence, April to July 1992

Kerry Sieh, Lucile Jones, Egill Hauksson, Kenneth Hudnut, Donna Eberhart-Phillips, Thomas Heaton, Susan Hough, Kate Hutton, Hiroo Kanamori, Anne Lilje, Scott Lindvall, Sally F. McGill, James Mori, Charles Rubin, James A. Spotila, Joann Stock, Hong Kie Thio, Jerome Treiman, Brian Wernicke, Judith Zachariasen

The Landers earthquake, which had a moment magnitude (M_w) of 7.3, was the largest earthquake to strike the contiguous United States in 40 years. This earthquake resulted from the rupture of five major and many minor right-lateral faults near the southern end of the eastern California shear zone, just north of the San Andreas fault. Its M_w 6.1 preshock and M_w 6.2 aftershock had their own aftershocks and foreshocks. Surficial geological observations are consistent with local and far-field seismologic observations of the earthquake. Large surficial offsets (as great as 6 meters) and a relatively short rupture length (85 kilometers) are consistent with seismological calculations of a high stress drop (200 bars), which is in turn consistent with an apparently long recurrence interval for these faults.

The Landers earthquake occurred at 11:58 universal time (UT) on 28 June 1992. Its seismic moment of 10^{27} dyne-cm is equivalent to a M_w of 7.3 (1). The earthquake resulted from right-lateral shear on five major faults, which have a total length of about 85 km, and several minor faults. Over 40,000 foreshocks, preshocks (2), and aftershocks to the Landers earthquake were recorded by the Southern California Seismographic Network (SCSN) in 1992.

The Landers earthquake sequence was generated by faults within an 80-km-wide belt of active right-lateral faults (3, 4) along the southern part of the eastern California shear zone (ECSZ) (Fig. 1). This zone of abundant seismicity and historical geodetic strain extends at least 500 km northwest from the San Andreas fault, through the Mojave Desert and beyond (5). The ECSZ is a major element of the transform plate boundary between the Pacific and North American plates and accommodates about 15% of the relative plate motion. The potential for large earthquakes within the ECSZ had been recognized well before the Landers earthquake [for example, (6, 7)].

K. Sieh, E. Hauksson, K. Hutton, H. Kanamori, A. Lilje, J. A. Spotila, J. Stock, H. K. Thio, B. Wernicke, and J. Zachariasen are at the Seismological Laboratory 252-21, California Institute of Technology, Pasadena, CA 91125. L. Jones, K. Hudnut, D. Eberhart-Phillips, T. Heaton, S. Hough, and J. Mori are at the U.S. Geological Survey, Pasadena, CA 91106. S. Lindvall is with Lindvall Richter Benuska Associates, Los Angeles, CA 90041. S. F. McGill is in the Department of Geological Sciences, California State University, San Bernardino, CA 92407. C. Rubin is at Central Washington State University, Ellensburg, WA 98926. J. Treiman is at the California Division of Mines and Geology, Los Angeles, CA 90012.

The large quantity of high-quality data from this earthquake provides an unusual opportunity to examine the source of a major earthquake. Abundant geological observations of surficial ruptures and excellent recordings by TERRAScope (8) and the 250 short-period seismic stations of the SCSN facilitate unprecedented comparisons of geological and seismological observations.

Preshocks, Foreshocks, and Mainshock

The Landers earthquake sequence began 2 months before its principal earthquake. At 02:25 UT on 23 April 1992, a M_L 4.6 earthquake occurred near Palm Springs, 8 km northeast of the San Andreas fault (Fig. 1). Because of its proximity to this fault, the U.S. Geological Survey declared a San Andreas Hazard Level C, on the basis of guidelines published in 1991 (9). This designation meant that the probability that this event would be a foreshock to a larger, destructive earthquake on the San Andreas fault within the next 3 days was estimated to be 1%. This was the first earthquake large enough and near enough to the San Andreas fault to trigger an alert since the development of the guidelines. At 04:50 UT, a M_w 6.1 earthquake originated at the same site (10). The larger magnitude of this

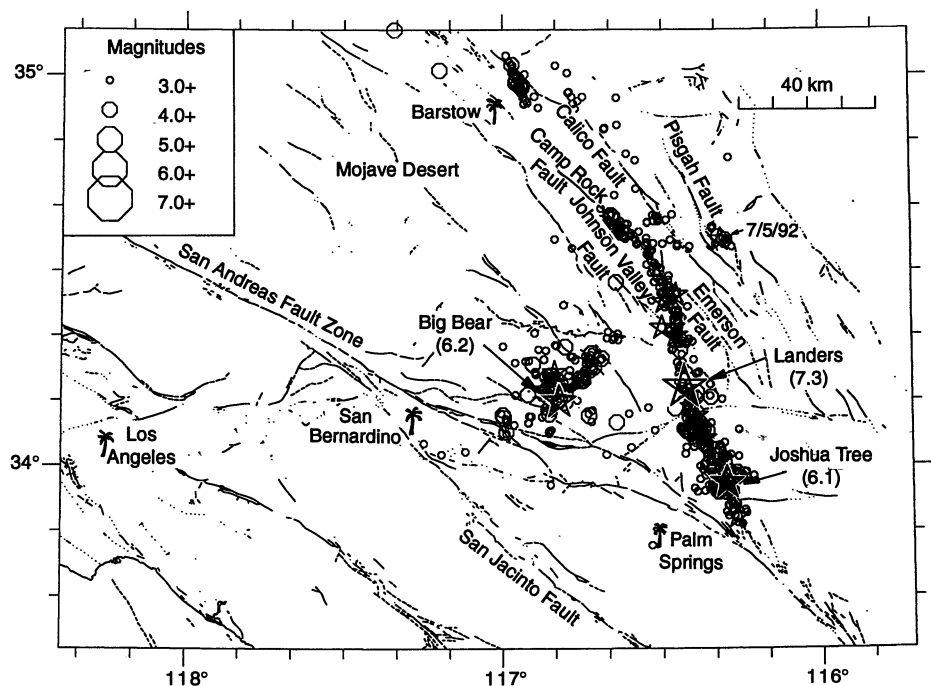


Fig. 1. Map of part of southern California, showing major active faults and earthquakes recorded from 1 January 1992 to 18 August 1992. Symbol size is proportional to magnitude. Earthquakes larger than M 5 are shown by stars; moment magnitudes are in parentheses. Faults are shown as dotted lines where concealed by deposits of Late Tertiary age, as dashed lines where inferred, and as solid lines where exposed.

earthquake, the Joshua Tree event, led to a San Andreas Hazard Level B, meaning that a 5 to 25% probability existed of a larger earthquake on the San Andreas fault within 3 days. However, no earthquake in the Landers sequence has clearly occurred on the San Andreas fault.

The Joshua Tree earthquake's short-period focal mechanism and its aftershock zone indicate that it originated on a 10- to 12-km-long dextral-slip fault that trends N10°W between the San Andreas and the Pinto Mountain faults (Fig. 2). Rupture propagation during the earthquake was northward (11), away from the San Andreas fault. The earthquake may have originated on the West Deception Canyon fault, one of several Quaternary, north-northwest-striking faults that diverge from the San Andreas fault just south of the Joshua Tree epicenter (12). However, aerial and ground reconnaissance in the days after the earthquake revealed no primary surficial fault ruptures.

In June, two tight clusters of aftershocks occurred north of the Pinto Mountain fault. The latter of the two clusters, a series of 25 small earthquakes (M 1.2 to 3.0), began at 07:21 UT on 28 June. Five hours later, at 11:58 UT, the Landers earthquake originated within this same small cluster of foreshocks, at 34°13'N, 116°26'W and a depth between 3 and 8 km (13).

Fault Ruptures During the Mainshock

The Landers earthquake was the result of dextral slip on several faults within a broad, 70-km-long zone (Fig. 3A). The trend of this zone is northward in its southern section and northwestward in its central and northern sections. Two primary characteristics of the fault zone are the right-stepping en echelon geometry of the principal faults and the predominance of dextral slip (Fig. 3, A and D). From south to north, the five principal faults of the mainshock are the Johnson Valley, Landers, Homestead Valley, Emerson, and Camp Rock faults (Fig. 3A). The total length of these overlapping fault strands is ~85 km. All but the Landers fault had been mapped before the earthquake (3, 7, 14). All of the Landers and most of the Homestead Valley faults ruptured during the earthquake, but only parts of the other faults were involved in this event. The northern two-thirds of the Johnson Valley fault, the southern two-thirds of the Emerson fault, and major parts of the Camp Rock fault did not slip during the earthquake sequence.

The Landers earthquake began on the Johnson Valley fault, several kilometers north of the fault's southern terminus. The southern Johnson Valley fault, the Landers

fault, and the nearby parts of the Homestead Valley fault all slipped more than 2 m locally (Fig. 3D). Offsets >3 m were typical along the central third of the Homestead Valley fault. Many localities along the Emerson fault had dextral offsets >4 m. A maximum slip of 6 m occurred at Galway Lake Road; this value equals those of the largest surficial strike-slip dislocations of the 20th century in the Western Hemisphere (15). Dextral offsets along the Camp Rock fault were mostly <1 m.

The Eureka Peak fault, south of the Johnson Valley fault, experienced surficial dextral offsets as large as 21 cm (16).

Although seismological records of the mainshock strongly suggest a unilateral rupture from the epicenter on the Johnson Valley fault northward, eyewitness accounts suggest initial surficial rupture of the Eureka Peak fault late in the mainshock (Fig. 3E). A M_w 5.7 aftershock, 3 min after the mainshock, was caused by rupture south of the Pinto Mountain fault, perhaps along the Eureka Peak fault.

Large vertical slip on major and secondary faults was common and in several places >1 m. Where they traverse older tectonic landforms, these new scarps generally represent an incremental growth of the older

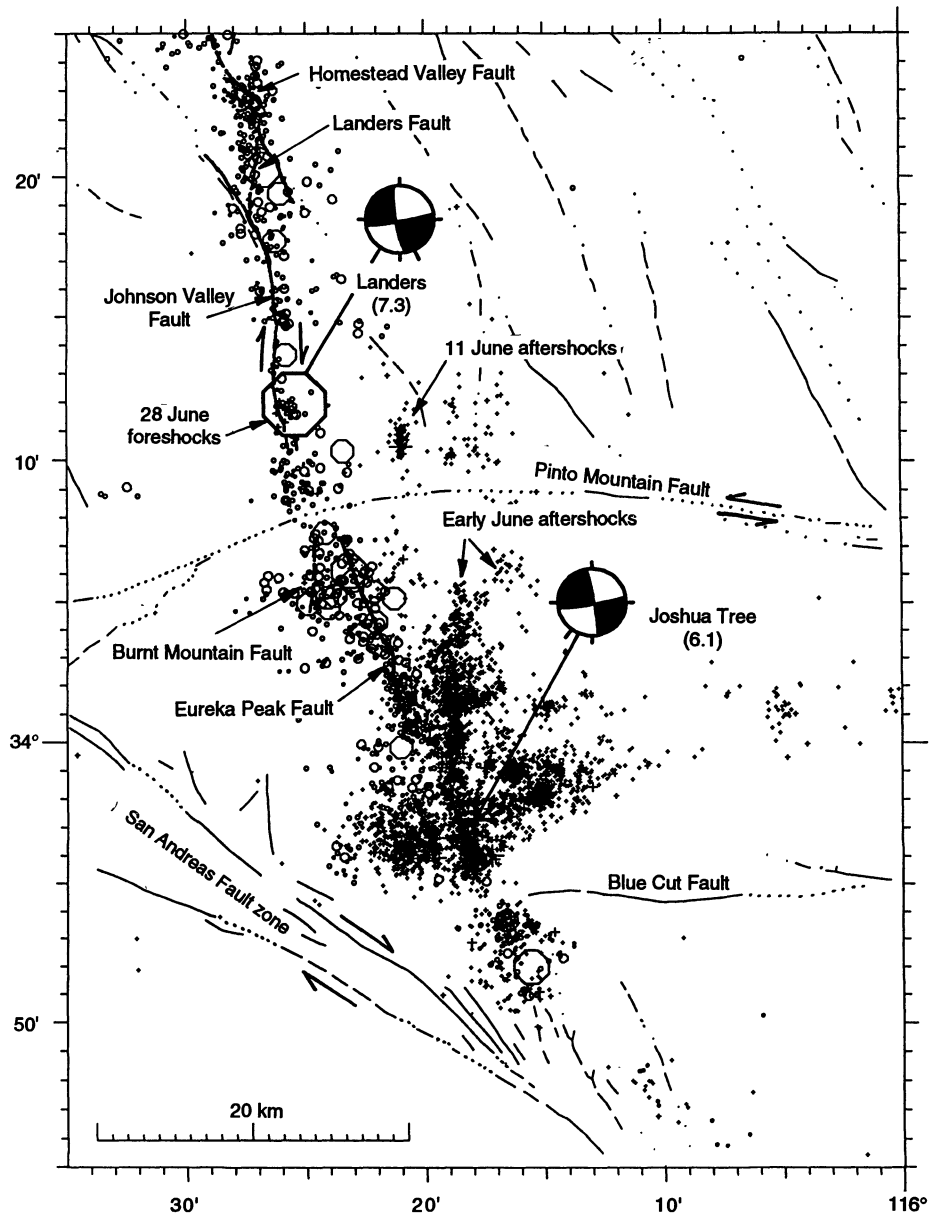


Fig. 2. Map of major active faults and seismicity recorded from January 1992 to 18 August 1992 in the Joshua Tree region. Earthquakes before the Landers mainshock are shown by small crosses; later events are shown by open circles; moment magnitudes are in parentheses. First-motion, lower hemisphere focal mechanisms are for the 23 April Joshua Tree M 6.1 and 28 June Landers M 7.3 earthquakes and show that these events produced mostly horizontal slip on near-vertical faults. The right-lateral, north-striking nodal planes are assumed to be the actual fault planes.

landforms. Some of the secondary faults reflect interaction of the five major faults. The thrust fault north of the intersection of the Landers and Homestead Valley faults, for example, seems to be the result of dextral slip on the Landers fault. This action has caused the block west of the Landers fault to overrun the Homestead Valley fault. The transfer of slip between the Homestead Valley and Emerson faults is accomplished by dextral slip on several intervening north-striking faults (Fig. 3A).

One surprising characteristic of surficial ruptures of the Landers earthquake is the subdued nature of small landforms that are attributable to earlier ruptures. These features are generally an order of magnitude less common and more degraded than landforms along the San Andreas fault, where ruptures recur about every one to two centuries (6). From this comparison, we estimate that the previous major ruptures of these faults occurred at least several thousand years ago.

Aftershocks

Aftershock epicenters clearly delineate a 95-km-long, arcuate, vertical structure that strikes N10°W in the south and N30°W in the north (Fig. 1). The aftershock zone extends 55 km north of the mainshock epicenter, but the surficial breaks extend 5 km further north (Fig. 3). The zone reaches 40 km south of the mainshock epicenter, a few kilometers north of the San Andreas fault and nearly coincident with the southern extent of the aftershocks of the Joshua Tree earthquake (Fig. 2). Thus, the aftershock zone extends 20 km south of the southernmost surficial break (Fig. 2). In the first few weeks of the sequence, the heaviest aftershock activity occurred in a band that is coincident with the trace of the Eureka Peak fault. The heavy aftershock activity and surficial afterslip on the Eureka Peak fault (16) indicate slippage on this fault after the mainshock.

Three hours after the mainshock, at 15:05 UT, the largest aftershock (so far) occurred 30 km west of Landers, near Big Bear Lake (Fig. 1). This moderate (M_w 6.2), damaging earthquake occurred on a vertical, northeast-striking left-lateral fault with its own aftershock zone that extended 10 to 15 km away from the San Andreas fault. In addition, a broad distribution of aftershocks extended away from the main rupture surface both to the north and to the south toward the San Andreas fault zone. Some of these aftershocks appear to have been on small northwest-striking faults that intersect the fault that caused the Big Bear earthquake. Although it originated on a separate fault, the Big Bear earthquake is considered an aftershock because it was within one fault length of the mainshock,

in an area that experienced stress changes during the mainshock that were conducive to failure (17), and because it fits within the temporal and magnitude distributions of the aftershocks (18). No surficial faulting accompanied the Big Bear earthquake, and no geologically mapped faults have been associated with the structure that produced the earthquake. The only mapped active fault in the vicinity of this northeast-striking left-lateral fault is the Santa Ana fault, an east-west-striking, north-dipping reverse fault (19).

One of the largest aftershocks (M_L 5.5 on 5 July) also had its own set of aftershocks and was located east of the Landers trend, on or near the Pisgah fault (Fig. 1). Another notable off-fault cluster began soon after the Landers mainshock, northeast of Barstow. The largest event in the group was a M_L 4.7 shock, which occurred 1 month after the trend started. The Barstow trend is approximately aligned with the main Landers aftershock zone and has raised speculation that a large aftershock could occur in the region between the main zone and the Barstow trend. Prior geological mapping, however, indicates no throughgo-

ing structure exists between these aftershocks and the Camp Rock fault (3, 4). Thus, if another large earthquake occurs in the near future near the Barstow aftershocks, it would likely involve rupture of the Calico fault ($M \leq 7.5$) (20).

In addition to nearby aftershocks, most of southern California and parts of Nevada have had an above-average incidence of earthquakes since the 28 June earthquake. Two M_L 5.6 earthquakes were apparently triggered by the Landers earthquake: the Little Skull Mountain earthquake on 29 June, 280 km to the northeast (21), and the Mojave earthquake on 11 July, 220 km to the northwest. The largest earthquake in the Los Angeles area was a M_L 3.9 event in Pasadena the day after the mainshock. These events would have been called aftershocks if they had occurred in a remote area without dense seismic recording. Microearthquake activity, mostly in volcanic regions, also increased at even greater distances (22).

The temporal development of the aftershocks during the first 9 weeks fits a well-described pattern (18). If this pattern continues, then additional aftershocks in the

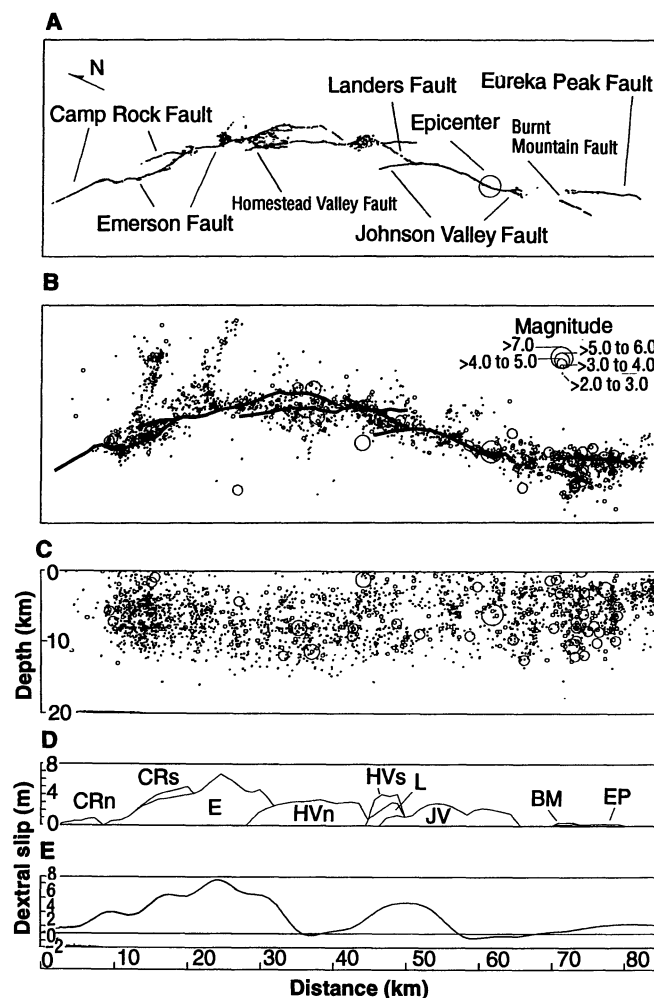


Fig. 3. Characteristics of the Landers earthquake. (A) Map view of surficial fault ruptures of the Landers earthquake. (B) Map view of seismicity recorded by the Southern California Seismographic Network from 28 June 1992 to 18 August 1992. (C) Vertical cross section of earthquakes in (B), projected onto the horizontal axes of the maps in (A) and (B). (D) Distribution of dextral surficial slip along the faults. Abbreviations: CRn, Camp Rock north; CRs, Camp Rock south; E, Emerson; HVn, Homestead Valley north; HVs, Homestead Valley south; L, Landers; JV, Johnson Valley; BM, Burnt Mountain; and EP, Eureka Peak. (E) Slip distribution along the fault zone calculated from TERRAScope record at Pasadena.

Landers and Big Bear zones greater than M 5 are probable (67% in 1993) and aftershocks greater than M 6 are still possible (14% in 1993).

Source Parameters

The short-period focal mechanism of the mainshock indicates that initial rupture was purely dextral on a steeply dipping fault that strikes $N10^\circ W$ (Fig. 2). The moment tensor of the Landers earthquake that was determined from teleseismic surface-wave data shows a focal mechanism that was similar to the first-motion mechanism and a total moment of 1.1×10^{27} dyne-cm. Teleseismic body-wave data can be fit by two distinct sources with 6- and 8-s durations and peaks ~ 10 s apart. The slip direction of the first source is almost identical to that of the short-period focal mechanism. The moment of the first source is 0.19×10^{27} dyne-cm; the second source is three times larger (0.61×10^{27} dyne-cm) and trends more westerly ($N30^\circ W$). The sizes of the earthquake that were determined with different techniques are quite similar (Table 1). The best estimate of the magnitude of the earthquake is the moment magnitude of 7.3 (23). The ratio of the energy to the moment is 4×10^{-14} and indicates an unusually high stress drop of 200 bars. The moment of the Big Bear aftershock is 2.8×10^{25} dyne-cm, equivalent to a magnitude of 6.2.

The Landers earthquake was recorded on six TERRAScope stations (8), all within 300 km of the mainshock. The seismograms at Goldstone to the north and Pinon Flat to the south (Fig. 4) show a strong directivity (11), consistent with unilateral rupture propagation to the north. The station in Pasadena is located 200 km west of the earthquake, perpendicular to the rupture direction. From its signal, we computed a slip-distribution function along the fault (24) (Fig. 3E). The local, broad-band data are consistent with the teleseismic results and indicate that the Landers earthquake consisted of two distinct subevents ~ 30 km apart. The second event originated north of the first and was about twice as large.

Discussion

The Landers earthquake sequence is consistent with current knowledge of the tectonics of southern California. Most of the faults that produced the mainshock had been mapped previously and were known to have dextral offsets. Furthermore, these faults are part of the ECSZ, a well-known belt of active strike-slip faults, geodetic strain, and abundant seismicity (3-7, 14, 25). The location and sense of slip of the coseismic faults are consistent with recent

tectonic models of the Mojave region (4, 26).

One unexpected characteristic of the Landers sequence is the mismatch of the termini of the Landers aftershock zone and the surficial rupture (Fig. 3). Aftershocks stop ~ 5 km south of the northern end of surficial rupture, near the northern end of the Emerson fault (Fig. 3). The paucity of aftershocks on the Camp Rock fault suggests that slip must be confined to the top few kilometers of the crust, a result also suggested by the geodetic signal at Goldstone (27). The lack of aftershocks on the northwestern 5 km of the Johnson Valley rupture and the southern Homestead Valley rupture might also indicate that these faults had only surficial offsets. Aftershocks extend 20 km south of the southern end of the mapped surficial fault breaks (Fig. 2). Because the analysis of the waveform data from the mainshock indicates unilateral northward rupture in the mainshock, the southern aftershocks may be occurring on faults activated only during the first aftershock and the Joshua Tree earthquake. Alternatively, the slip south of the mainshock may be too small to be resolved from

the available mainshock waveforms. Extension of the Johnson Valley fault southward in the subsurface across the Pinto Mountain fault would require interpenetration of two major active fault zones.

Another unexpected characteristic of the earthquake is the nearly simultaneous failure of several discrete large faults. Although such behavior has occurred elsewhere (28), it has been rare in California. In that state, it has been more common for entire faults to rupture, as in the 1987 Superstition Hills earthquake, or for individual or contiguous segments of major faults to fail coseismically. The involvement of more than one major fault in the production of this earthquake complicates the use of fault or fault-segment length in the prediction of the size and frequency of future earthquakes. For example, in Wesnousky's evaluation of earthquake hazards in California, the relatively short length of faults in the Landers area led to estimates of M 6.9 or less for earthquakes on the faults that broke during the Landers earthquake (6). One consequence of these estimates was his probable overestimation of the frequency of events in the region. However, the effects of underestimating magnitude and overestimating frequency counteract each other in the creation of probabilistic maps of shaking hazard. Wesnousky estimated that this part of the Mojave Desert has high (0.2 to 0.6) probabilities of a damaging earthquake (peak ground acceleration $\geq 0.1g$) in the 50 years after 1986. In hindsight, of course, we see that this conclusion was accurate. Future probabilistic hazard estimates can be improved by consideration of rupture dynamics and better paleoseismic information that allow evaluation of the likelihood of one fault rupture to trigger seismic slip on another fault or fault segment.

The similarity between the seismologically and the geologically determined seismic moments and slip distributions for the Landers earthquake suggests that the fault slip at the surface during the earthquake is comparable to the average slip at depth (29). In contrast, recent smaller California earthquakes (30) have significantly smaller surficial offsets than the coseismic slip calculated from their seismic moment. Therefore, the surficial slip necessary to produce mappable surficial landforms and offsets along many active faults in California may occur primarily during earthquakes $>M$ 7.

Damage from the Landers earthquake was light despite its large magnitude, primarily because of its remote location and the geometry of the source. The maximum shaking in an earthquake occurs in the region of maximum moment release, which in this case was along the Emerson fault, ≥ 30 km from the nearest dwelling. Because

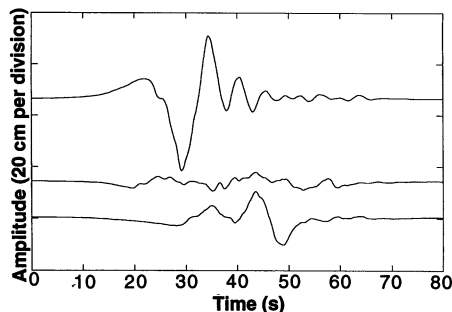


Fig. 4. Seismograms of the M_w 7.3 Landers mainshock recorded at TERRAScope stations at Goldstone (top trace, 125 km $N16^\circ W$ of the epicenter), Pinon Flat (middle trace, 68 km $S2^\circ W$ of the epicenter), and Pasadena (bottom trace, 161 km $S88^\circ W$ of the epicenter).

Table 1. Magnitude estimates of the Landers earthquake.

Data source	Amplitude magnitude	Moment*	Moment magnitude
Surface waves	7.6	1.1	7.3
Body waves		0.8	7.3
Geologic moment†		0.9	7.3
Geodetic moment (37)		1.0	7.3
Local seismograms	6.8	1.0	7.3‡

*Times 10^{27} dyne-cm. †The geologic moment is calculated from an assumed fault width of 15 km and a rigidity of 3.3×10^{11} dyne cm^{-2} . ‡Energy magnitude derived from local seismograms (38).

of its unilateral northward rupture, much of the energy of the earthquake was directed away from the few communities near the southern part of the fault. Such light damage should not be considered typical of a M 7.3 earthquake in California. In addition, the two M_L 5.6 earthquakes triggered by the Landers event at distances of 200 to 300 km raise the possibility that a major earthquake on the San Andreas fault, outside most of the Los Angeles metropolitan region, could spawn aftershocks in more heavily populated regions (31).

The subdued tectonic landforms along the faults that ruptured during the Landers earthquake indicate that an earlier major surface rupture or ruptures on these faults occurred at least a few millennia ago. This observation is consistent with indirectly estimated recurrence intervals, which are derived by division of a fraction of the geodetic rate of shear across the ECSZ into the slip during this particular earthquake. These recurrence intervals contrast markedly with those of the San Andreas fault, which are typically one or more centuries, not several millennia. This long interval may be physically related to the high stress drop of the Landers earthquake (32).

Several researchers have proposed that the elastic strains caused by the Landers earthquake have brought much of the southern San Andreas fault closer to failure (17, 33). Moreover, the rate of moderate to large earthquakes in southern California has increased in the last decade, so that the probabilities of larger earthquakes have increased as well (34). Thus, earthquakes on the southern San Andreas fault should now be considered more likely, and potential precursors should be carefully evaluated.

The probability that an earthquake near the San Andreas fault will be a foreshock to a San Andreas earthquake has been derived (35) and depends on three factors: the long-term probability of the mainshock, the rate of background seismicity, and the rate at which foreshocks precede mainshocks. The first two factors have changed because of the Landers earthquake. The long-term probability has increased by an unknown amount because of the change in stress on the San Andreas fault, which increases the probability that an earthquake will be a foreshock. The rate of background activity, however, has also increased because of the occurrence of Landers aftershocks near the fault, and so decreases the probability of an earthquake acting as a foreshock. The rate of aftershocks decays with time, so the effect of the second factor will decrease with time. Immediately after the Landers earthquake, the probability that a M 6 earthquake near the San Andreas fault would be a foreshock to a major earthquake was smaller than it was before the Landers event

(for instance, for the Joshua Tree earthquake). An increase by a factor of 1000 in the probability of a resulting mainshock would be needed to make a M 6 event as likely to be a foreshock as it had been before the Landers earthquake. Six months after the Landers earthquake, the long-term probability of an earthquake on the San Andreas fault would have to increase by a factor of 5 for the probability of a M 6 event being a foreshock to reach its pre-Landers value (36).

REFERENCES AND NOTES

1. The National Earthquake Information Center (NEIC) gave the earthquake a 20-s surface-wave magnitude (M_s) of 7.6. Magnitudes calculated from seismic moment [T. Hanks and H. Kanamori, *J. Geophys. Res.* **84**, 2348 (1979)] are considered more representative of the size of an earthquake than M_s values and are preferentially used for earthquakes above M 6 in this article. Local magnitudes (M_L) are used for earthquakes smaller than M 6.
2. "Foreshock" and "preshock" are not standardized terms. We restrict "foreshock" to events that, as with aftershocks, are closely tied to the mainshock in time and space. L. Jones [*Bull. Seismol. Soc. Am.* **75**, 1669 (1985)] defined immediate foreshocks as those events that occur within 5 days and 10 km of the mainshock. "Preshock" is used for events that occur over greater temporal and spatial scales but that seem necessarily related.
3. T. Dibblee, Jr., Geologic map of the Rodman Mountains quadrangle, San Bernardino County, CA, *U.S. Geol. Surv. Misc. Geol. Invest. Map I-430* (1964); Geologic map of the Emerson Lake quadrangle, San Bernardino County, CA, *U.S. Geol. Surv. Misc. Geol. Invest. Map I-490* (1967); Geologic map of the Old Woman Springs quadrangle, San Bernardino County, CA, *U.S. Geol. Surv. Misc. Geol. Invest. Map I-518* (1967); Geologic map of the Joshua Tree quadrangle, San Bernardino and Riverside counties, CA, *U.S. Geol. Surv. Misc. Geol. Invest. Map I-516* (1967).
4. R. K. Dokka, *Geology* **11**, 305 (1983); _____ and C. J. Travis, *Tectonics* **9**, 311 (1990).
5. J. Sauber et al., *J. Geophys. Res.* **91**, 12683 (1986); J. Savage et al., *Geophys. Res. Lett.* **17**, 2113 (1990).
6. S. G. Wesnousky, *J. Geophys. Res.* **91**, 12587 (1986).
7. E. W. Hart et al., "Summary Report," *Calif. Div. Mines Geol. Open-File Rep. 88-1* (1988); R. E. Wallace, "General Features," *U.S. Geol. Surv. Prof. Pap. 1515* (1990).
8. TERRAScope is a network of six high-dynamic-range (240 dB), broad-band (20 Hz to dc) digital seismographic stations, funded by the L. K. Whittier and Arco foundations at the California Institute of Technology [H. Kanamori et al., *Eos* **72**, 564 (1991)].
9. L. M. Jones et al., "Short-term earthquake alerts for the southern San Andreas fault," *U.S. Geol. Surv. Open-File Rep. 91-32* (1991).
10. The M_s of the Joshua Tree earthquake was 6.1 and its moment from surface waves was 1.7×10^{25} dyne-cm, which corresponds to a M_w of 6.1. This earthquake had an extensive aftershock sequence, with >6000 recorded events before the Landers earthquake. The most distinctive feature of the aftershock sequence is that the rate of aftershocks did not begin to decay until almost 2 days after the Joshua Tree mainshock.
11. The rupture direction is recognized from the directivity of the event's seismograms. If earthquake rupture propagates toward a station, the duration of the wave train at that station is shortened and ground motions are more severe because the later arrivals have a shorter distance to travel to

the station. In turn, a station located away from the propagation direction will record less severe ground motions.

12. M. Pymer, *Eos* **73**, 363 (1992).
13. The depth of the mainshock is not well constrained because of the sparse distribution in the region of stations in the seismic network. This estimate is based on revised locations computed with a regionally specific velocity model.
14. R. E. Crippen, thesis, University of California, Santa Barbara (1989); M. W. Manson, *Calif. Div. Mines Geol. Fault Eval. Rep. FER-180* (1986); F. S. Riley and J. Moyle, *Calif. Dep. Water Resour. Bull. 91-2* (1960). We have named one of the major, previously unrecognized and unnamed faults the Landers fault, after the nearest town and the name of the earthquake.
15. This value is approximately equal to the largest documented offset along the San Andreas fault in 1906 and along the Fairweather fault, Alaska, in 1958.
16. The Eureka Peak fault (and nearby Burnt Mountain fault) have been named and described by J. Treiman ["Landers earthquake of June 28, 1992, San Bernardino County, CA: field trip guidebook," *Southern California Section of the Association of Engineering Geologists Annual Field Trip* (1992)].
17. R. S. Stein, G. C. P. King, J. Lin, *Science* **258**, 1328 (1992).
18. P. A. Reasenberg and L. M. Jones [*ibid.* **243**, 1173 (1989)] showed that the rate at which aftershocks occur after mainshocks, λ , can be described by

$$\lambda(t, M) = 10^{[a + b(M_m - M)](t + c)^{-p}}$$

where t is time, M is magnitude of an aftershock, M_m is the magnitude of the mainshock, and a , b , c , and p are constants. The overall productivity of the sequence is represented by a , b is the relative frequency of large to small magnitudes, p is the rate at which the aftershocks decay with time, and c is the time delay until the sequence starts to decay. Once these four parameters are determined for a sequence, the rate of aftershocks can be fully described and the probability of future aftershocks determined. The parameters for Landers are almost exactly average for California aftershock sequences:

Event	Parameter			
	a	b	c	p
Landers	-1.86	0.88	0.05 day	0.97
California average	-1.76	0.91	0.05 day	1.08

If the aftershocks to the Big Bear earthquake are considered as separate from the Landers aftershocks, the rate of M 3 to M 4 aftershocks at Big Bear underpredicts the rate of $\geq M$ 5 aftershocks from this event, and the rate of M 3 to M 4 aftershocks at Landers overpredicts the rate of $\geq M$ 5 aftershocks at Landers.

19. J. Matti et al., *U.S. Geol. Surv. Open-File Rep. 92-354* (1992).
20. This magnitude estimate is based on standard relations between magnitude and fault length (θ).
21. For example, S. Brockman et al., *Eos* **73**, 354 (1992).
22. The distant triggering of earthquakes by the Landers mainshock is discussed in detail by P. A. Reasenberg and colleagues [*ibid.*, p. 392] and by D. P. Hill and co-workers (unpublished results).
23. The local magnitude scale saturates at $-M$ 6.8 and is, therefore, an inadequate measure of the energy of such a large event. Surface-wave magnitudes from NEIC are known to be high for California mainshocks because of a low-attenuation path between California and Europe (D. J. Wald et al., *Bull. Seismol. Soc. Am.*, in press).
24. If we assume a one-dimensional line-source model, the slip distribution is derived from the seismogram at Pasadena by deconvolving the Joshua Tree seismogram from the Landers seismogram

- and assuming a rupture velocity of 3 km s^{-1} and a depth of faulting of 15 km; this method is described by H. Kanamori *et al.* [*Geophys. Res. Lett.* **19**, 2267 (1992)].
25. L. K. Hutton *et al.*, *Calif. Geol.* **33**, 110 (1980).
 26. R. Dokka and C. Travis, *Geophys. Res. Lett.* **17**, 1323 (1990).
 27. Y. Bock *et al.*, *Nature* **361**, 337 (1993); G. Blewitt *et al.*, *ibid.*, p. 340.
 28. Some examples are the 1932 $M 7.4$ Cedar Mountain, Nevada, the 1932 $M 7.5$ Chang Ma, China, the 1891 $M 8$ Nobi, Japan, the 1954 $M 7.2$ Fairview Peak–Dixie Valley, Nevada, and the 1957 Gobi-Altai, Mongolia, earthquakes.
 29. This similarity is based on the assumption that the average depth to the base of the fault zone is the maximum depth of aftershocks, 15 km.
 30. These events include the 1979 $M 6.5$ Imperial Valley, the 1984 $M 6.2$ Morgan Hill, the 1986 $M 5.9$ North Palm Springs, the 1987 $M 6.6$ Superstition Hills, and the 1989 $M 6.9$ Loma Prieta earthquakes.
 31. However, the three well-known major San Andreas earthquakes (1857, 1906, and 1989) did not produce large off-fault aftershocks and had small aftershock sequences compared with those of other California events [low value of a in the equation in (18)]. Therefore, strong concerns about off-fault aftershocks may be unwarranted.
 32. Slow-moving faults may have higher stress drops because they are more irregular and have had more time to strengthen between events [H. Kanamori and C. R. Allen, in *Earthquake Source Mechanics*, S. Das and C. H. Scholz, Eds. (American Geophysical Union, Washington, DC, 1986), vol. 6, pp. 566–574].
 33. R. A. Harris and R. W. Simpson, *Nature* **360**, 251 (1992); S. C. Jaumé and L. R. Sykes, *Science* **258**, 1325 (1992).
 34. The rate of earthquakes from 1945 to 1984 has been compared with that from 1985 to the summer of 1992. The rate of occurrence of $\geq M 4$ earthquakes did not change, but the relative distribution of magnitudes changed significantly, with larger earthquakes more common in the later period. This difference implies an increase by a factor of 6, to 12% per year, in the probabilities of a $M 7$ earthquake in southern California.
 35. D. C. Agnew and L. M. Jones, *J. Geophys. Res.* **96**, 11959 (1991).
 36. L. M. Jones, *Eos* **73**, 357 (1992).
 37. From Global Positioning System data collected at 13 sites by the U.S. Geological Survey, Southern California Earthquake Center, and the California Department of Transportation; processed by the U.S. Geological Survey and the Southern California Earthquake Center. The inversion was tested for slip on a four-segment geometry with varied location and was well-determined and stable for total moment results, yielding a range of 0.9×10^{27} to 1.1×10^{27} dyne-cm (K. Hudnut *et al.*, *ibid.*, p. 365).
 38. The radiated energy estimated with TERRAScope by the method described by H. Kanamori and co-workers (*Bull. Seismol. Soc. Am.*, in press) is 4.3×10^{29} ergs, which corresponds to the energy radiated by a $M_L 7.3$ earthquake if M_L did not saturate. See also H. Kanamori and colleagues in (24).
 39. We thank D. Agnew, A. Densmore, J. Dolan, K. Gross, D. Jackson, S. Larsen, M. Lisowski, M. Rymer, Z. Shen, and J. Svarc for helpful discussions and assistance. We also thank the seismic analysts of the Southern California Seismographic Network who have processed the Landers earthquake data, including R. Dollar, R. Geary, D. Given, W. Huston, S. Perry-Huston, R. Robb, and L. Wald. Data collection and processing partially supported by the Caltech Earthquake Research Affiliates Emergency Earthquake Fund and by the Southern California Earthquake Center (contribution number 25), which is funded by the National Science Foundation and the U.S. Geological Survey. Additional support from Division of Geological and Planetary Sciences, California Institute of Technology (contribution number 5217).

A Nickel Metal Hydride Battery for Electric Vehicles

S. R. Ovshinsky, M. A. Fetcenko, J. Ross

Widespread use of electric vehicles can have significant impact on urban air quality, national energy independence, and international balance of trade. An efficient battery is the key technological element to the development of practical electric vehicles. The science and technology of a nickel metal hydride battery, which stores hydrogen in the solid hydride phase and has high energy density, high power, long life, tolerance to abuse, a wide range of operating temperature, quick-charge capability, and totally sealed maintenance-free operation, is described. A broad range of multi-element metal hydride materials that use structural and compositional disorder on several scales of length has been engineered for use as the negative electrode in this battery. The battery operates at ambient temperature, is made of nontoxic materials, and is recyclable. Demonstration of the manufacturing technology has been achieved.

The interest in electrically powered vehicles extends nearly as far back as interest in vehicles powered by hydrocarbon fuels. Throughout this period, however, there has been a major technological barrier to the development of practical electric vehicles (EVs) that can compete in performance and cost with those that use internal combustion (IC) engines. This barrier has been the lack of an economical battery with sufficient energy density and other essential performance criteria. In this article, we describe the science and technology of a nickel metal hydride (NiMH) battery that will permit future EVs to replace IC-powered vehicles in many applications.

S. R. Ovshinsky and M. A. Fetcenko are at Energy Conversion Devices, Inc., 1675 West Maple Road, Troy, MI 48084. J. Ross is in the Chemistry Department, Stanford University, Palo Alto, CA 94305, and consultant to Energy Conversion Devices, Inc.

Recently, U.S. federal and state governments have been providing an impetus for the development of an EV industry through legislation aimed at increasing national energy independence and reducing the impact of automobile emissions on the environment. California has passed laws that demand that 2% of new cars sold in 1998 be emission-free, and this percentage is slated to grow to 10% by the year 2003; 12 eastern states are planning similar laws. A comprehensive energy bill passed by Congress contains a tax credit for EV buyers. This bill also requires state and federal governments to purchase alternative-fuel fleet vehicles, with the percentage of new, cleaner fuel vehicles growing to 90% by the year 2000. It is expected that EVs will make up an increasing portion of alternative fuel vehicles as the market grows.

There are several important advantages

of EVs compared with IC-powered vehicles. First, EVs are emission-free: they produce no pollution during operation. This quality is particularly important in city centers where congested automobile traffic is the primary source of local air pollution. The overall unwanted emissions that result from combustion of fossil fuels for the generation of electricity are also far less per mile of EV travel than the emissions produced directly by a fossil fuel-powered car. This fact, discussed in detail in a study by the Electric Power Research Institute (EPRI) (1), results from the sophisticated emissions controls that can be used economically by large, efficient, central power-generation facilities. Second, the EPRI study also details how the primary energy efficiency of electric transportation can exceed the efficiency of gasoline-powered vehicles in many instances. For example, the study shows that electric-powered commercial fleet vans that are used in urban areas have a significant advantage in energy efficiency over their gasoline-powered counterparts, traveling about 1100 miles per barrel of oil consumed at the power plant compared with 620 miles per barrel of oil refined into gasoline. This difference results primarily from the higher energy efficiency of power plant combustion—approximately twice as high as combustion of gasoline in an IC engine in urban traffic. Third, conversion from cars directly powered by fossil fuel to ones powered by electricity can shift the choice of hydrocarbon fuels that are consumed in the United States from oil to coal and gas. This change could possibly reduce the oil imports and, consequently, reduce the U.S. trade imbalance and the strategic vulnerability of its energy supply. Photovoltaic and other renewable energy sources are